

Suspended graphene membranes to control Au nucleation and growth

Joachim Dahl Thomsen¹, Kate Reidy¹, Thang Pham¹, Julian Klein¹, Anna Osherov², Rami Dana¹, Frances M. Ross¹

¹Department of Materials Science and Engineering, Massachusetts Institute of Technology, Cambridge, Massachusetts 02139, USA

²Department of Electrical Engineering and Computer Science, Massachusetts Institute of Technology, Cambridge, Massachusetts 02139, USA

Abstract:

Control of nucleation sites is an important goal in materials growth: nuclei in regular arrays may show emergent photonic or electronic behavior, and the nucleation density influences parameters such as surface roughness, stress, and defects such as grain boundaries once the nuclei coalesce into thin films. Tailoring substrate properties to control nucleation is therefore a powerful tool for designing functional thin films and nanomaterials. Here, we examine nucleation control for metals deposited on two-dimensional (2D) materials, focusing on how the condition of the surface determines the nucleation parameters and the resulting structure. Through quantification of faceted, epitaxial Au island nucleation on graphene, we show that ultra-low nucleation densities with nuclei several micrometers apart can be achieved by changing the nature of the support beneath the 2D material to create suspended 2D membranes and eliminating extraneous nucleation sites. Our data highlight the extreme sensitivity of metal nucleation and diffusion on graphene to extrinsic factors and suggest new avenues for applications where long diffusion distances of metals on graphene are required, such as self-assembly of epitaxial nanoparticle arrays or patterning of metals using areas of suspended graphene with low density of nucleation sites.

1. Introduction

In the initial stages of metal deposition, atoms diffuse on the target surface and aggregate to form islands.¹ Patterning the sites at which the metal islands nucleate is a powerful strategy for self-assembly of nanostructure arrays with plasmonic or electronic properties.^{2, 3, 4} In the absence of deliberate or unintended heterogeneous nucleation sites, nucleation occurs at random with a density determined by the atom diffusivity and flux.¹ As the nuclei coalesce to form a thin film, the nucleation density determines parameters such as film stress, the density and nature of grain boundaries and grain crystallography^{5, 6, 7} that are critical for metal thin films in advanced microelectronic, optical, and magnetic devices.⁸ Depositing the metal on a 2D material surface

provides opportunities for controlling nucleation over large, step-free areas and hence tailoring the structure and properties of both island arrays and coalesced thin films for applications such as color generation,³ energy devices,⁹ and biosensing.¹⁰ Exfoliated 2D materials can achieve lateral length scales of ~ 1 mm,¹¹ while sizes of 2D materials grown by chemical vapor deposition can extend across an entire wafer-scale growth substrate. Graphene is particularly interesting because the morphology of metals on graphene appears to be tunable via the substrate on which the graphene is placed. Metals deposited then annealed on SiO₂-supported mono- or few-layer graphene (both referred to here as Gr) show island number density that depends on the number of graphene layers, with lower density for thicker Gr.¹²⁻¹⁵ The mechanism of this effect may be related to the observation that surface strain variations and roughness affect Au diffusion on graphite and Gr surfaces.¹⁶ Understanding these phenomena in detail would enable nucleation tuning for metals on 2D surfaces and hence optimized strategies for fabricating functional materials. We are particularly interested in controlling nucleation on suspended (free-standing) Gr, i.e. Gr that is not in direct contact with a substrate. Suspended Gr (and other suspended 2D materials) are promising for applications such as catalyst support.^{17, 18} They also offers advantages for understanding metal diffusion and nucleation more generally, since eliminating the substrate can reveal the intrinsic interaction between metal and 2D material.

However, studies of intrinsic nucleation phenomena on suspended Gr are hindered by the presence of contamination from sample preparation methods,^{19, 20, 21} hydrocarbons and adsorbed water from ambient air,²² or tape residues used in the exfoliation process.¹⁶ These act as heterogeneous nucleation sites for metals. On bulk graphite, heterogeneous sites are known to influence metal nucleation.^{22, 23} The lowest Au nucleation densities on graphite, in the range $1-10 \mu\text{m}^{-2}$, were achieved by cleaving in ultra-high vacuum (UHV) conditions^{22, 23} or by annealing air-cleaved graphite in UHV conditions at 600 °C for several hours.²⁴ Such values match well with reported defect densities in natural graphite.²⁵⁻²⁷

Here, we study Au diffusion and nucleation on suspended Gr that is free of most extrinsic nucleation sites usually arising from contamination and avoids any influence of the substrate. We show that clean suspended Gr has remarkably different nucleation properties compared to Gr supported on a substrate. Suspended Gr displays Au nucleation density orders of magnitude lower than supported graphene. Furthermore, the nucleation density is thickness-dependent, decreasing with increased thickness and attaining values similar to those seen for Au nucleation on clean bulk graphite.²²⁻²⁴ Analysis of these results suggest that, in the absence of extrinsic nucleation sites,

surface roughness determines the nucleation and diffusion characteristics for Au on Gr. We discuss two benefits of the low nucleation density on suspended Gr: patterning metals on a Gr surface using through a substrate with regions of suspended and supported Gr, and the opportunities for self-assembly of epitaxial nanoparticles by defect engineering of nucleation sites.⁴

2. Results and Discussion

2.1 Ultra-low and layer-dependent Au nucleation density on suspended Gr

We first discuss nucleation of Au on Gr and the conditions under which particularly low nucleation density occurs. Figure 1 shows the results of depositing Au on Gr after a sample preparation, cleaning and deposition process described in Methods. The Gr was transferred onto a SiN membrane with holes so that the Gr is free-standing or “suspended” over the holes but “supported” by SiN between holes. An overview of such samples is given in Fig. S1. Figure 1a, b shows transmission electron microscopy (TEM) and scanning TEM (STEM), respectively, of an exfoliated Gr crystal 3 layers (L) in thickness while Fig. 1c shows thicker (10L) Gr. In each image, both suspended and supported regions are visible. The images show a strikingly lower nucleation density (N) of Au on suspended Gr compared to supported Gr. In Fig. 1b the SiN-supported region has $N_{3L, \text{supp}} \sim 110 \mu\text{m}^{-2}$, compared to $N_{3L, \text{susp}} = 1.6 \mu\text{m}^{-2}$ in the suspended region. We find reproducibly that N is significantly lower on suspended compared to supported Gr. We also find that thicker Gr has lower N : in Fig. 1c a 10L thick suspended Gr area did not nucleate any Au, demonstrating diffusion lengths greater than the hole radius ($\sim 1 \mu\text{m}$).

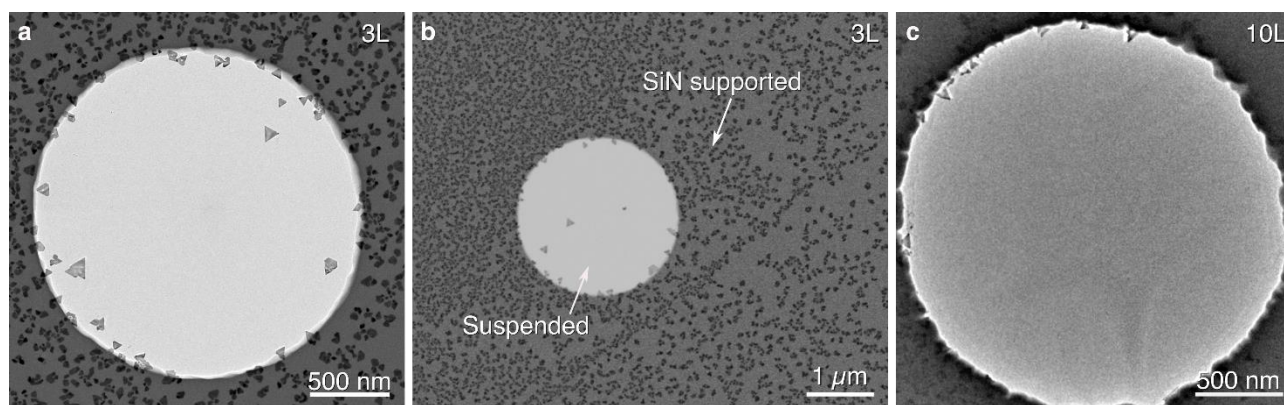


Figure 1: Low nucleation density on suspended Gr compared to SiN supported Gr. (a, b) TEM and lower magnification high angle annular dark field STEM images of 3L Gr with 0.3 nm Au. The contrast in (b) has been inverted to make it easier to compare the images. (c) TEM image of 10L Gr. No nucleation of Au was visible on the suspended areas but rather on the edge of the hole and on the supported regions. Note the weak diffraction contrast in (c) arising from bending of the

membrane.

The ultralong diffusion lengths shown in Fig. 1 emphasize the importance of eliminating contamination arising from the exfoliation, transfer method, or ambient air to avoid distorting measurements of N by extrinsic nucleation sites. Our sample preparation procedure, described in Methods, combines UHV deposition conditions, a specific polymer used as handle for the transfer, and sample annealing prior to evaporation, to create suspended Gr samples that are sufficiently clean for these measurements. Imaging is carried out directly after Au deposition with no post-growth anneal.

Having established methods for obtaining ultralow N in suspended Gr, we investigate Au nucleation and diffusion in greater detail using samples in which the transferred Gr crystal is made up of regions of varying thickness. Figure 2 shows measurements as a function of Gr layer number after depositing Au on clean, suspended Gr. The Au has formed well-dispersed, compact, and faceted islands with N clearly varying with layer number. Figure 2a shows images of Au islands nucleated on 1L, 2L, and 4L suspended Gr. Figure 2b shows histograms of the Au island area on the corresponding layer thicknesses across the entire sample. The island shapes vary, but for context, a triangular island with area $6 \cdot 10^3 \text{ nm}^2$ has an edge length of 118 nm. In Fig. 2c, d we plot the layer-dependent N and the average island area for several samples. We see a decreasing trend for N with $N_{1L}=7.8 \mu\text{m}^{-2}$ as average for monolayer Gr, while for membranes thicker than 5L, $N_{>5L}=0.8 \mu\text{m}^{-2}$. Measurements of the values of N for thicker membranes are limited by the hole diameter, as in Fig. 1b. However, the values obtained are still comparable to literature values of $N=1-10 \mu\text{m}^{-2}$ on clean bulk graphite with UHV deposition conditions.²²⁻²⁴ Thicker substrates, as in the very thick graphite in the lower right region of Fig. S2, appear to show values of N that are similar to the value at 5-8L. In the following we, therefore, treat $N_{>5L}=N_{\infty}=0.8 \mu\text{m}^{-2}$ as reference for N on bulk graphite.

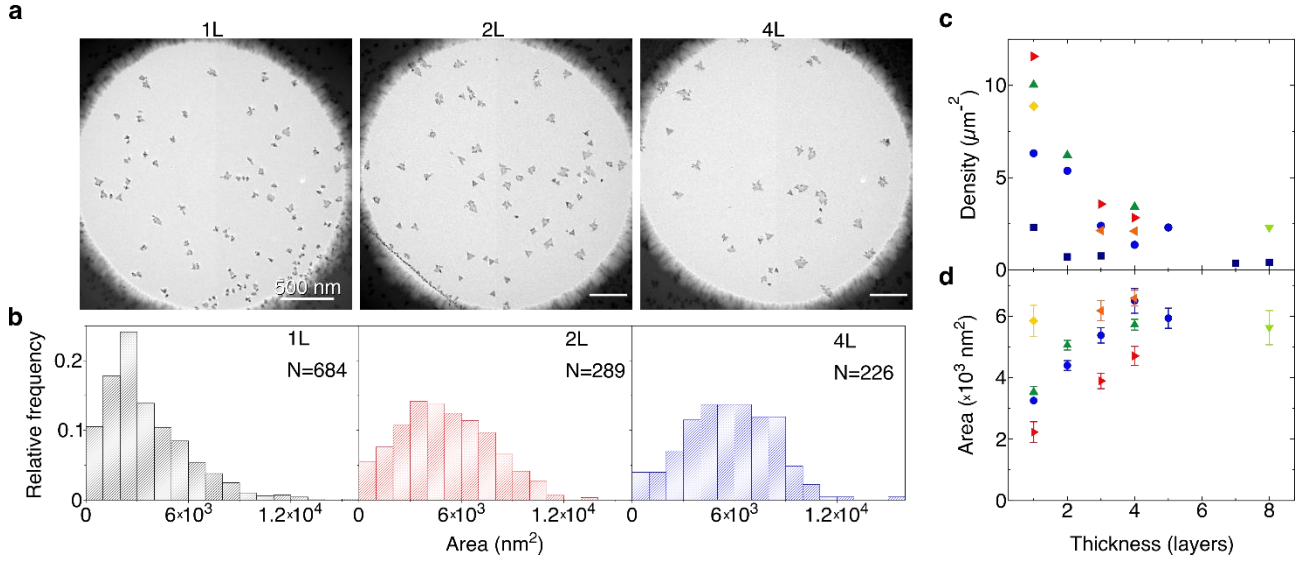


Figure 2: Layer dependent Au deposition characteristics on Gr. (a) TEM images of Au deposited on suspended 1L, 2L, and 4L Gr that are all from the same sample. (b) Histograms of Au areas from the sample shown in (a). The island areas were measured over several holes, at each of which the Gr thickness is known. The combined areas measured were 72, 39, and 79 μm^2 for 1L, 2L, and 4L Gr, respectively. (c) Au nucleation density on suspended Gr plotted against Gr thickness. The six different symbol colors/shapes correspond to six different samples. See Methods for details on nucleation density measurements. (d) Average island area plotted against Gr thickness for each sample and each thickness. The error bars indicate the standard error. One sample in (c) (dark blue, square data points) was not plotted in (d) due to challenges in measuring the island areas, see Methods. That sample is shown in Figure S2.

In line with the procedure of previous studies we can use mean-field diffusion theory to estimate the diffusion constant of Au on our samples.^{12, 16} Since the flux of Au atoms from the evaporator is constant onto all regions of the sample, we can estimate the difference in Au diffusivity when comparing results for different layer numbers using¹

$$N \propto \left(\frac{1}{D}\right)^{\frac{i}{i+2.5}} \quad (2)$$

where i is the critical nucleus size of Au on Gr and D is the Au diffusivity. Using $N_{1L}=7.8 \mu\text{m}^{-2}$ and $N_{\infty}=0.8 \mu\text{m}^{-2}$ for the nucleation density on suspended monolayer Gr and bulk graphite, respectively, and assuming $i=1$ and 2 (Ref. 16), results in $\frac{D_{1L}}{D_{\infty}} = 3 \cdot 10^{-4}$ and $6 \cdot 10^{-3}$, respectively. Hence, we estimate that the Au diffusivity on monolayer suspended Gr is 2-3 orders of magnitude lower than D_{∞} . We can also compare the Au diffusivity on suspended and SiN-

supported Gr. From Fig. 1b we had $N_{3L, \text{supp}} \sim 110 \mu\text{m}^{-2}$ and $N_{3L} = 1.6 \mu\text{m}^{-2}$. This results in $\frac{D_{3L, \text{supp}}}{D_{3L, \text{susp}}} = 4 \cdot 10^{-7}$ and $7 \cdot 10^{-5}$ with $i=1$ and 2 , respectively, a difference of 4-6 orders of magnitude. Thus, the difference in Au diffusivity is significantly greater when comparing suspended and supported Gr against suspended monolayer Gr and bulk graphite. Given the stark difference in N between suspended and supported Gr, as shown in Fig. 1b, this suggests that areas with different thin film properties can be created through substrate modification in certain areas to create suspended regions. This may lead to metal patterning with opportunities discussed further in Section 3.

To explain the observed layer dependence of N , we first consider a model in which charge transfer between Au and Gr is proposed to drive a layer thickness-dependent variation in island size that was observed.¹³ However, this model applies for islands that are smaller than in our case, where the side lengths of the Au islands are in the range 70-120 nm for 1-8L Gr, significantly larger than the Au islands that typically form on supported Gr.¹²⁻¹⁶ This indicates a mechanism different from charge transfer to explain the thickness-dependent variations in N in our samples. Furthermore, since our N for >5L thick suspended Gr is comparable to reported defect densities in natural graphite,²⁵⁻²⁷ this suggests that the factors which increase N for monolayer Gr and thin few-layer Gr crystals are largely eliminated at 5L thickness.

Instead, we suggest that our observed layer dependence on N is consistent with an explanation related to a decrease in surface roughness with thickness. Surface roughness has been shown to affect adatom diffusion on Gr,¹⁶ because diffusion is lowered or increased by compressive or tensile strains respectively.^{29, 30} Roughness can therefore increase N because regions with compressive strain, and thus lower Au diffusivity, will act as effective concentrators of adatoms and hence nucleation centers. The root mean square (RMS) surface roughness of monolayer Gr supported on SiO₂ or SiN has been reported to be between 0.19-0.35 nm,³¹⁻³⁵ with this relatively high value the result of the substrate not being atomically smooth. On the other hand, suspended monolayer Gr is known to exhibit intrinsic roughness with slightly lower RMS values, on the order of only 0.1 nm,³⁶⁻³⁹ and furthermore, the roughness of suspended few-layer Gr decreases as the number of layers increases.⁴⁰ Thus, situations of lower roughness correspond to the circumstances of smaller N . This applies to our observations of increased Au diffusivity as both on suspended Gr compared to supported Gr and as the layer thickness increases. The hypothesis that roughness determines N

(in the absence of heterogeneous nucleation sites) provides guidance on tuning or patterning the condition of the 2D material surface to optimize N of the deposited metal for a given application.

2.2 Effect of contamination, adsorbed water, and ripples on Au nucleation

So far, we have considered Au nucleation and diffusion processes on pristine Gr. We now discuss the effects of extraneous nucleation sites, including how they alter Au morphology as well as nucleation density. To obtain the largest Au diffusivity and the intrinsic value of N , extraneous sites should of course be eliminated. In our samples the typical sources of extraneous nucleation are polymer residue from the transfer process, adsorbed water from exposure to ambient air, and wrinkles in the suspended membrane, especially for monolayer graphene.

We find that nucleation on clean Gr typically results in faceted and epitaxially aligned islands with diameters ~ 100 nm, as shown in Fig. 3a. This is consistent with previous reports for Au on bulk graphite.^{22, 23} The diffraction pattern in Fig. 3b shows that the (111) plane of the face centered cubic Au structure is parallel to the Gr(0001) plane and the Au[220] direction is parallel to the Gr[10-10] direction. Prior studies have typically assigned the growth mode of Au on graphite as diffusion limited aggregation, sometimes with a less than unity sticking coefficient to account for more compact dendrite formation.⁴¹ However, with our deposition temperature around 100 °C we find faceted islands that more closely resemble the thermodynamically expected morphology as modelled by the Winterbottom shape of Au on Gr.⁴² The compact nature of the islands also shows that Au adatoms easily diffuse around the island once they attach to it.⁸

We find that this Au island morphology is extremely sensitive to surface contamination.^{22, 24} Islands affected by contamination are readily visible in TEM images, as in Fig. 3a, where Au islands that nucleated on contamination are typically very small with a diameter on the order of 10 nm. Larger flat triangular nanocrystals surround these regions. We attribute the smaller islands to Au that landed within the contaminated region, with the larger islands supplied by diffusion of Au adatoms across the clean Gr. Fig. 3c shows that Au islands nucleated on and around contamination orient randomly with respect to the Gr support, unlike the epitaxial triangular islands. Hence, it is possible to estimate which Au islands nucleated on polymer residue, helping to optimize cleaning and deposition protocols.

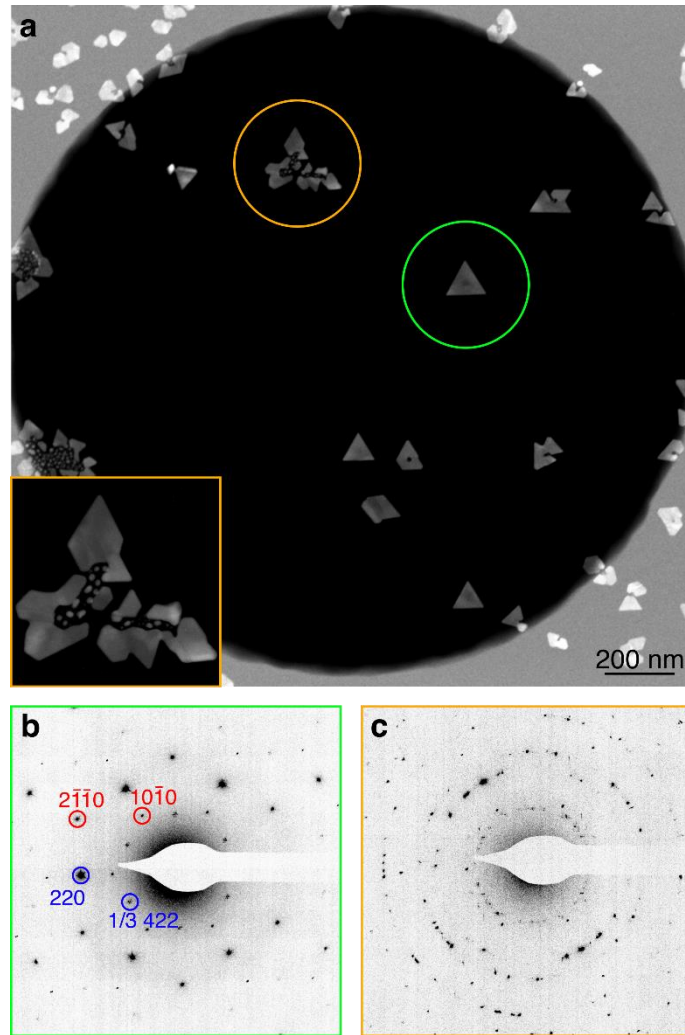


Figure 3: Epitaxy of Au on clean suspended Gr. (a) TEM image of 3L Gr with deposited Au. The green and orange circle marks the extent of the selected area aperture used to capture the diffraction patterns in (b) and (c), respectively. The inset in (a) shows an enlarged view of the region indicated in orange. In (b) the red indices are for Gr and the blue are for Au.

The samples we have discussed so far were annealed in UHV to temperatures above 500 °C immediately prior to deposition. Such vacuum annealing is presumed to remove polymer residues from the transfer process as well as adsorbed water. To examine annealing effects, in Fig. 4 we show the result of exfoliating Gr crystals onto an SiO₂ substrate then depositing Au without annealing. Au deposition on supported monolayer Gr (Fig. 4a) results in $N=500 \mu\text{m}^{-2}$, and the island morphology is less faceted as compared to our annealed samples. N has been measured by others at $\sim 1200 \mu\text{m}^{-2}$ for room temperature deposition on SiO₂-supported monolayer Gr.¹⁶ Our depositions take place at around 100 °C and at lower rate, so our lower N is consistent with this result. To evaluate how annealing affects deposition onto thicker layers, we show in Fig. 4b Au

deposited on 128 nm thick graphite which was subsequently transferred to a TEM grid for imaging. The Au has the same epitaxial relation to the graphite as is shown in Fig. 3b, albeit with larger rotational variance, as evidenced by the diffuse diffraction spots shown in the inset of Fig. 4b. The value of $N=150 \mu\text{m}^{-2}$. Thus, both monolayer and bulk have significantly higher N than the suspended samples (which were annealed), and the high N cannot be attributed to the substrate because it is seen even on the thick 2D crystal.

These results show that annealing is a necessary step in the preparation of low- N surfaces for epitaxy. Furthermore, we attribute the increased N on the samples shown in Fig. 4 compared to their vacuum annealed counterparts in Fig. 1-3 to adsorbed water from ambient air which does not evaporate simply upon inserting the sample in UHV. This conclusion is in line with previous studies of Au nucleation on graphite.²⁴ It is interesting to note that standard metal evaporators do not allow for annealing the sample prior to metal deposition. However, given the striking effect on metal diffusion lengths and epitaxy, it would be interesting to study the effect of removing adsorbed water on the key physical properties of the metal-2D material interface, particularly the electrical contact resistance.

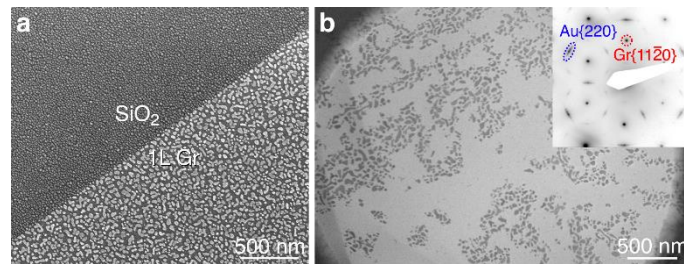


Figure 4: Au deposition on un-annealed samples. (a) SEM image of Au evaporation on an as-exfoliated monolayer Gr crystal on SiO₂. (b) TEM image of Au deposited on 128 nm thick graphite while it was supported on SiO₂ and subsequently transferred to a TEM grid for TEM imaging. The inset shows a diffraction pattern with Gr indexes in red and Au in blue font.

We finally discuss the origin of correlated heterogeneous nucleation sites. We occasionally have observed Au islands that have nucleated in lines as seen in Fig. 5. (We excluded holes with such lines from our nucleation density analysis, as described in Methods.) We see that several of these lines of Au are continuous across different holes although not directly visible on the supported regions due to the large nucleation density there. This suggests that these are static ripples, or possibly ripplocations in the Gr,^{43, 44} arising due to the mechanical transfer process or thermal expansion during annealing. These lines were primarily observed on monolayer Gr, suggesting

that the increased stiffness and stability of thicker crystals may hinder the formation of ripples. Control of nucleation sites therefore also requires attention to possible stresses caused by the transfer process.

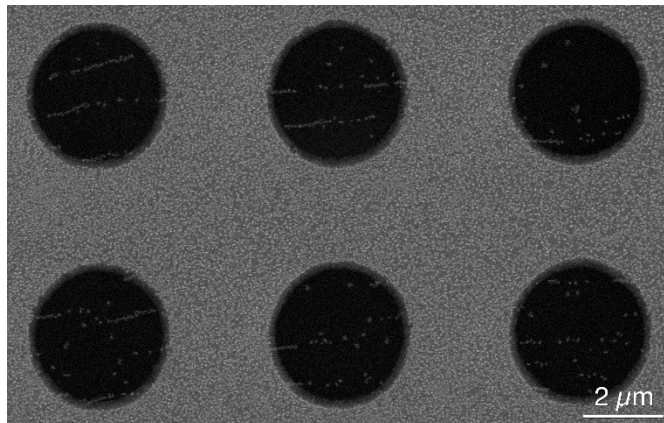


Figure 5: *Ripples in monolayer Gr. Scanning electron microscopy overview image of monolayer Gr on which 0.3 nm Au has been deposited.*

3 Conclusions and Outlook

By measuring Au nucleation and diffusion characteristics on Gr that has been prepared to minimize heterogeneous nucleation sites, we have shown that the nucleation density of Au on suspended Gr is significantly lower than on supported Gr. We furthermore find that the Au nucleation density on suspended Gr decreases with increasing layer thickness. The suppression of nucleation can be dramatic: for Gr crystals thicker than 5L it is possible to create suspended areas with zero Au nucleation events surrounded by dense arrays of islands. This indicates diffusion distances exceeding the hole radius of 1 μm, and an enhancement in diffusion distance of several orders of magnitude compared to the supported surface outside the hole. In the absence of extrinsic nucleation sites such as polymer contamination or adsorbed water, we argue that surface roughness is the main factor determining Au diffusivity. We have described a method to obtain ultra-clean suspended Gr and shown how to identify Au nucleation on extraneous nucleation sites using TEM imaging.

Understanding the role of roughness, strain, contamination, and deposition conditions, particularly temperature, is necessary for full control of metal island and film morphology on Gr and provides opportunities for novel fabrication methods. The large difference in Au diffusivity for suspended and supported Gr could be interesting for creating films with laterally varying properties. Our results suggest that it might be possible to create a coalesced film on supported Gr but have a

discontinuous film on suspended Gr, without the need for lithographic patterning methods on the graphene surface. This may be the case if the lateral width of the film region is smaller than the intrinsic nucleation separation. The ultralong diffusion distance of suspended few-layer Gr also offers additional opportunities. A deliberate introduction of nucleation sites through means such as focused ion beam irradiation at a period smaller than the intrinsic nucleation separation could enable self-assembly of epitaxial islands only at specified locations and without the need for optical or electron beam lithography.⁴ We anticipate that the diffusion and nucleation characteristics can further be controlled by changing the substrate temperature during evaporation; by tuning the conditions we would expect longer diffusion distances at elevated temperatures.

Methods

Sample fabrication: Gr was obtained by exfoliation of natural graphite (NaturGrafit GmbH, Germany) onto oxygen plasma-treated substrates of 90 nm thick SiO₂ on Si using 3M Magic scotch tape. We identified suitable crystals using optical microscopy, mapping regions of different thickness (layer number) from their contrast, see Fig. S1a. We then transferred the crystals onto either homemade TEM-compatible sample grids as shown in Fig. S1b or “location tagged” TEM grids from Norcada, Inc., Canada. The homemade grids consist of 300 nm thick SiN membrane windows with multiple ~3 μm diameter holes etched in the window. The Norcada TEM grids have a 200 nm thick SiN membrane with several 2 μm holes. Placement of the crystals on the grids was achieved using wedging transfer,⁴⁵ a method based on the use of cellulose acetate butyrate (CAB) as polymer handle. After transfer we bake the samples for 1 minute at 140 °C to improve the adhesion between the transferred crystals and the substrate. Then we dissolve the CAB in acetone for 15 minutes and dry the samples using critical point drying. This procedure has previously been shown to yield close to completely clean suspended Gr after vacuum annealing to temperatures >500 °C for >1 hour⁴⁶ and faceted Au nanoislands.⁴⁷

Au deposition: Prior to evaporation we anneal the samples at 500 °C overnight in a vacuum chamber that also contains the Au evaporator. Without breaking vacuum, we evaporate Au using home-built thermal evaporators. We measure the deposition rate using a quartz crystal microbalance and deposit typically 0.3 nm at a rate of 0.1 nm/min. However, the power needed to get this deposition rate varies 5-10% between many experiments. Due to the small distance of about 1 cm between the sample and the evaporator we expect radiation from the evaporator to heat up the sample during evaporation: measurements using a thermocouple suggest a sample temperature of about 100 °C during evaporation. Hence, we expect some variation in the sample

temperature across experiments which may explain the observed variation in N seen in Fig. 2c. The pressure during evaporation is typically in the range $5\text{-}9 \times 10^{-9}$ Torr.

Electron microscopy: After deposition, we removed the samples from the vacuum system and imaged *ex situ* in either TEM, STEM, or SEM to quantify the deposition morphology at suspended regions of different layer thickness; supported regions could also be imaged through the silicon nitride at lower resolution using TEM or STEM. We used a JEOL 2010F TEM operated at 200 kV for TEM imaging and a FEI Themis STEM also operated at 200 kV for STEM imaging. SEM imaging was performed in a Zeiss Gemini 450 SEM.

Data analysis: To calculate N for each sample, we add all the hole areas with the same thickness Gr across them and divide by the number of islands nucleated over these holes. This simple count is modified by several factors: (1) A small number of Au islands in our samples appear to have nucleated on contamination, as shown in Fig. 3. The density of such islands does not appear to depend strongly on layer number. To avoid bias when calculating N (Fig. 2), we count the cluster of Au islands nucleated on contamination as one island. We expect that the islands nucleated on contamination alter the overall value of N slightly but not the layer thickness-dependent trend observed. (2) In cases where we observe Au nucleated along lines that may be step edges (see the bulk Gr in Fig. S2) or wrinkles in thin Gr (see Fig. 5), we exclude the hole from the count. (3) In one sample (Figure S2) the islands had dendritic shapes and the areas could not be calculated readily by our image processing algorithm. This is the sample that was excluded from Fig. 2d. Such variations in island geometry may be due to changes in experimental conditions due for example to small changes in evaporator power; we expect, in general, a higher evaporation rate or lower substrate temperature to result in dendritic growth.⁴¹ The layer dependent nucleation density on SiN supported Gr is complicated by geometric factors described in SI Section 2.

Acknowledgements

J.D.T. acknowledges support from Independent Research Fund Denmark through Grant Number 9035-00006B. The authors acknowledge use of the MRSEC Shared Experimental Facilities at MIT, supported by the National Science Foundation under award number DMR-1419807, and use of the MIT.nano Characterization Facilities. K.R. acknowledges funding and support from a MIT MathWorks Engineering Fellowship and ExxonMobil Research and Engineering Company through the MIT Energy Initiative.

REFERENCES

- [1] Venables, J.A.; Spiller, G.D.T. Nucleation and Growth of Thin Films. In *Surface Mobilities on Solid Materials*; Binh, V. T., Eds; Springer: Boston, **1983**, pp 341-404.
- [2] Whitesides, G.M; Grzybowski, B. Self-assembly at all scales. *Science* **2002**, 295, 2418-2421.
- [3] Kristensen, A.; Yang, J.K.; Bozhevolnyi, S.I.; Link, S.; Nordlander, P.; Halas, N.J.; Mortensen, N.A. Plasmonic colour generation. *Nat. Rev. Mater.* **2016**, 2, 1-14.
- [4] Zarubin, V.; Reidy, K.; Yu, Y.; Charaev, I.; Thomsen, J. D.; Klein, J.; Ross, F. Controlling the Nucleation of Metal Nanoislands on Two-dimensional Materials via Focused Ion Beam Patterning. *Microsc. Microanal.* **2021**, 27.S1, 342-345.
- [5] Michely, T.; Krug, J. *Islands, mounds and atoms*. Springer **2004**.
- [6] Ratsch, C.; Venables, J. A. Nucleation theory and the early stages of thin film growth. *J. Vac.*
- [7] Doerner, M.F; Nix, W.D.; Stresses and deformation processes in thin films on substrates. *Crit. Rev. Solid State Mater. Sci.* **1988**, 14, 225-268.
- [8] Zhang, Z.; Lagally, M. G. Atomistic processes in the early stages of thin-film growth. *Science* **1997**, 276, 377-383.
- [9] Tiwari, J.N.; Tiwari, R.N; Kim, K.S. Zero-dimensional, one-dimensional, two-dimensional and three-dimensional nanostructured materials for advanced electrochemical energy devices. *Prog. Mater. Sci.* **2012**, 57, 724-803.
- [10] Estevez, M.C.; Otte, M.A.; Sepulveda, B.; Lechuga, L.M. Trends and challenges of refractometric nanoplasmonic biosensors: A review. *Anal. Chim. Acta* **2014**, 806, 55-73.
- [11] Huang, Y.; Pan, Y.H.; Yang, R.; Bao, L.H.; Meng, L.; Luo, H.L.; Cai, Y.Q.; Liu, G.D.; Zhao, W.J.; Zhou, Z; Wu, L.M. Universal mechanical exfoliation of large-area 2D crystals. *Nat. Commun* **2020**, 11, 1-9.
- [12] Zhou, H.; Qiu, C.; Liu, Z.; Yang, H.; Hu, L.; Liu, J.; Yang, H.; Gu, C.; Sun, L. Thickness-dependent morphologies of gold on N-layer graphenes. *J. Am. Chem. Soc.* **2010**, 132, 944-946.
- [13] Luo, Z.; Somers, L. A.; Dan, Y.; Ly, T.; Kybert, N. J.; Mele, E.; Johnson, A. C. Size-selective nanoparticle growth on few-layer graphene films. *Nano Lett.* **2010**, 10, 777-781.
- [14] Zhou, H.; Yu, F.; Chen, M.; Qiu, C.; Yang, H.; Wang, G.; Yu, T.; Sun, L. The transformation of a gold film on few-layer graphene to produce either hexagonal or triangular nanoparticles during annealing. *Carbon* **2013**, 52, 379-387.
- [15] Zhou, H.-Q.; Yu, F.; Yang, H.-C.; Chen, M.-J.; Wang, G.; Sun, L.-F. High-throughput thickness determination of n-layer graphenes via gold deposition. *Chem. Phys. Lett.* **2011**, 518, 76-80.

- [16] Liu, L.; Chen, Z.; Wang, L.; Polyakova, E.; Taniguchi, T.; Watanabe, K.; Hone, J.; Flynn, G. W.; Brus, L. E. Slow gold adatom diffusion on graphene: effect of silicon dioxide and hexagonal boron nitride substrates. *J. Phys. Chem. B* **2013**, 117, 4305–4312.
- [17] Julkapli, N. M.; Bagheri, S. Graphene supported heterogeneous catalysts: an overview. *Int. J. Hydrogen Energy* **2015**, 40, 948-979.
- [18] Antolini, E. Graphene as a new carbon support for low-temperature fuel cell catalysts. *Appl. Catal., B* **2012**, 123, 52-68.
- [19] Zan, R.; Bangert, U.; Ramasse, Q.; Novoselov, K. S. Evolution of gold nanostructures on graphene. *Small* **2011**, 7, 2868–2872.
- [20] Zan, R.; Bangert, U.; Ramasse, Q.; Novoselov, K. S. Metal-graphene interaction studied via atomic resolution scanning transmission electron microscopy. *Nano Lett.* **2011**, 11, 1087–1092.
- [21] Lin, Y. C.; Lu, C. C.; Yeh, C. H.; Jin, C.; Suenaga, K.; Chiu, P. W. Graphene annealing: how clean can it be? *Nano Lett.* **2012**, 12, 414-419.
- [22] Metois, J.; Heyraud, J.; Takeda, Y. Experimental conditions to obtain clean graphite surfaces. *Thin Solid Films* **1978**, 51, 105–117.
- [23] Darby, T.; Wayman, C. Nucleation and growth of gold films on graphite: I. Effects of substrate condition and evaporation rate. *J. Cryst. Growth* **1975**, 28, 41–52.
- [24] Anton, R.; Schneidereit, I. In situ TEM investigations of dendritic growth of Au particles on HOPG. *Phys. Rev. B* **1998**, 58, 13874.
- [25] Yang, R. T.; Wong, C. Kinetics and mechanism of oxidation of basal plane on graphite. *J. Chem. Phys.* **1981**, 75, 4471–4476.
- [26] Chang, H.; Bard, A. J. Formation of monolayer pits of controlled nanometer size on highly oriented pyrolytic graphite by gasification reactions as studied by scanning tunneling microscopy. *J. Am. Chem. Soc.* **1990**, 112, 4598–4599.
- [27] Tracz, A.; Wegner, G.; Rabe, J. P. Scanning tunneling microscopy study of graphite oxidation in ozone-air mixtures. *Langmuir* **2003**, 19, 6807–6812.
- [28] Thomsen, J.D.; Reidy, K.; Pham, T; Ross, F. Nucleation and Growth of Metal Films and Nanocrystals on Two-dimensional Materials. *Microsc. Microanal* **2020**, 26.S2, 1094-1096.
- [29] Ratsch, C.; Seitsonen, A. P.; Scheffler, M. Strain dependence of surface diffusion: Ag on Ag (111) and Pt (111). *Phys. Rev. B* **1997**, 55, 6750.
- [30] Brune, H.; Bromann, K.; Röder, H.; Kern, K.; Jacobsen, J.; Stoltze, P.; Jacobsen, K.; Norskov, J. Effect of strain on surface diffusion and nucleation. *Phys. Rev. B* **1995**, 52, R14380.

- [31] Geringer, V.; Liebmann, M.; Echtermeyer, T.; Runte, S.; Schmidt, M.; Rückamp, R.; Lemme, M. C.; Morgenstern, M. Intrinsic and extrinsic corrugation of mono-layer graphene deposited on SiO₂. *Phys. Rev. Lett.* **2009**, 102, 076102.
- [32] Ishigami, M.; Chen, J.; Cullen, W.; Fuhrer, M.; Williams, E. Atomic structure of graphene on SiO₂. *Nano Lett.* **2007**, 7, 1643–1648.
- [33] Cullen, W. G.; Yamamoto, M.; Burson, K. M.; Chen, J.-H.; Jang, C.; Li, L.; Fuhrer, M. S.; Williams, E. D. High-fidelity conformation of graphene to SiO₂ topographic features. *Phys. Rev. Lett.* **2010**, 105, 215504.
- [34] Xue, J.; Sanchez-Yamagishi, J.; Bulmash, D.; Jacquod, P.; Deshpande, A.; Watanabe, K.; Taniguchi, T.; Jarillo-Herrero, P.; LeRoy, B. J. Scanning tunnelling microscopy and spectroscopy of ultra-flat graphene on hexagonal boron nitride. *Nat. Mater.* **2011**, 10, 282–285.
- [35] Yamamoto, M.; Einstein, T. L.; Fuhrer, M. S.; Cullen, W. G. Charge inhomogeneity determines oxidative reactivity of graphene on substrates. *ACS Nano* **2012**, 6, 8335–8341.
- [36] Thomsen, J. D.; Gunst, T.; Gregersen, S. S.; Gammelgaard, L.; Jessen, B. S.; Mackenzie, D. M.; Watanabe, K.; Taniguchi, T.; Bøggild, P.; Booth, T. J. Suppression of intrinsic roughness in encapsulated graphene. *Phys. Rev. B* **2017**, 96, 014101.
- [37] Singh, S. K.; Neek-Amal, M.; Costamagna, S.; Peeters, F. M. Thermomechanical properties of a single hexagonal boron nitride sheet. *Phys. Rev. B* **2013**, 87, 184106.
- [38] Gao, W.; Huang, R. Thermomechanics of monolayer graphene: Rippling, thermal expansion and elasticity. *Mech. Phys. Solids* **2014**, 66, 42.
- [39] Ramírez, R.; Chacón, E.; Herrero, C. P. Anharmonic effects in the optical and acoustic bending modes of graphene. *Phys. Rev. B* **2016**, 93, 235419.
- [40] Meyer, J. C.; Geim, A.; Katsnelson, M.; Novoselov, K.; Obergfell, D.; Roth, S.; Girit, C.; Zettl, A. On the roughness of single- and bi-layer graphene membranes. *Solid State Commun.* **2007**, 143, 101–109.
- [41] Wynblatt, P.; Metois, J.; Heyraud, J. Modeling the growth of dendrite-like gold islands on graphite substrates. *J. Cryst. Growth* **1990**, 102, 618–628.
- [42] Reidy, R.; Thomsen, J. D.; Lee, H. Y.; Zarubin, V.; Yu, Y.; Wang, B.; Pham, T.; Ross, F. M. Quasi-van der Waals epitaxy of 3D metallic nanoislands on suspended 2D materials. **2021** (*in preparation*)
- [43] Kushima, A.; Qian, X.; Zhao, P.; Zhang, S.; Li, J. Ripplations in van der Waals layers. *Nano Lett.* **2015**, 15, 1302–1308.

- [44] Gruber, J.; Lang, A. C.; Griggs, J.; Taheri, M. L.; Tucker, G. J.; Barsoum, M. W. Evidence for bulk ripplocations in layered solids. *Sci. Rep.* **2016**, 6, 1–8.
- [45] Schneider, G. F.; Calado, V. E.; Zandbergen, H.; Vandersypen, L. M.; Dekker, C. Wedging transfer of nanostructures. *Nano Lett.* **2010**, 10, 1912–1916.
- [46] Thomsen, J. D.; Kling, J.; Mackenzie, D. M.; Bøggild, P.; Booth, T. J. Oxidation of Suspended Graphene: Etch Dynamics and Stability Beyond 1000°C. *ACS nano*2019,13, 2281–2288.
- [47] Reidy, K.; Varnavides, G.; Thomsen, J. D.; Kumar, A.; Pham, T.; Blackburn, A. M.; Anikeeva, P.; Narang, P.; LeBeau, J. M.; Ross, F. M. Direct imaging and electronic structure modulation of moiré superlattices at the 2D/3D interface. *Nat. Commun.* **2021**, 12, 1-9.

Supplementary information:

Suspended graphene membranes to control Au nucleation and growth

Joachim Dahl Thomsen¹, Kate Reidy¹, Thang Pham¹, Julian Klein¹, Anna Osherov², Rami Dana¹, Frances M. Ross¹

¹Department of Materials Science and Engineering, Massachusetts Institute of Technology, Cambridge, Massachusetts 02139, USA

²Department of Electrical Engineering and Computer Science, Massachusetts Institute of Technology, Cambridge, Massachusetts 02139, USA

Section 1. Sample overview

Figure S1a shows an optical microscopy image of as-exfoliated graphene (Gr) with different layer thicknesses across the crystal, as identified by the contrast to the bare SiO₂ substrate (see inset).

Figure S1b shows the crystal after transfer onto a homemade TEM-compatible sample grids.

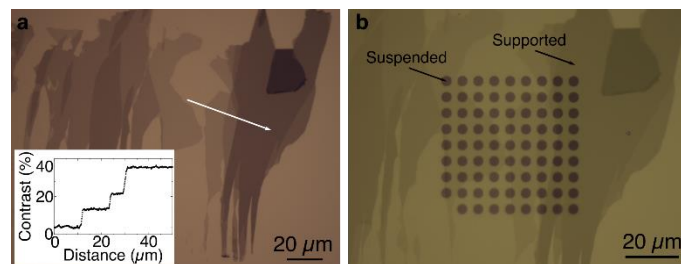


Figure S1: Sample overview. (a) Optical microscopy of an as-exfoliated Gr crystal with different thicknesses. The inset shows the contrast, $C(x) = (I_{BG} - I(x))/I_{BG}$, where I_{BG} is the average grey value of the bare SiO₂ substrate, and $I(x)$ is the grey value along the white arrow in (a). The contrast increases in multiples of about 11%, showing that the sample consists of 1, 2, and 4L thick Gr. (b) The crystal from (a) transferred to our homemade TEM sample grids. The original optical image from (a) is overlaid on the image of the transferred crystal and made transparent. This makes it easier to identify which layer thickness is present at each hole, due to lower contrast on SiN.

Section 2. Nucleation density on SiN-supported graphene

Figure S2 and S3 shows overview images of two samples. Figure S2a-c and Fig. S2a,b show the Gr before and after transfer, while Fig. S2d and Fig. S3c are stitched TEM and SEM images, respectively, showing the entire sample. In Fig. S2d Au particles appear as bright speckles both on the suspended and supported Gr, while in Fig. S3c the Au particles appear as dark speckles due to the different imaging mode used. The nucleation density in the suspended regions varies consistently as a function of layer thickness, see Fig. 2c in the main text. However, we find that that Au density on the SiN-supported Gr is inhomogeneous across the sample. For instance, in Fig. S3c there are two regions with 4L Gr. The lower of the two regions has a nearly coalesced film of Au while the nucleation density in the upper region is sparser. Also, within the 8L region in Fig. S2d, the upper part has a higher nucleation density than the lower part. This makes the determination of nucleation density layer dependency challenging for supported Gr. We believe that geometrical effects may have a particularly strong effect on Au diffusion on supported Gr in our samples. The placement of the Gr crystal across the holes, and the positional relation between the step edges, which act as a sink and possible blocking site for Au by nucleating a row of Au islands, may cause longer range spatial variations in nucleation density on supported Gr that drown out the layer dependence.

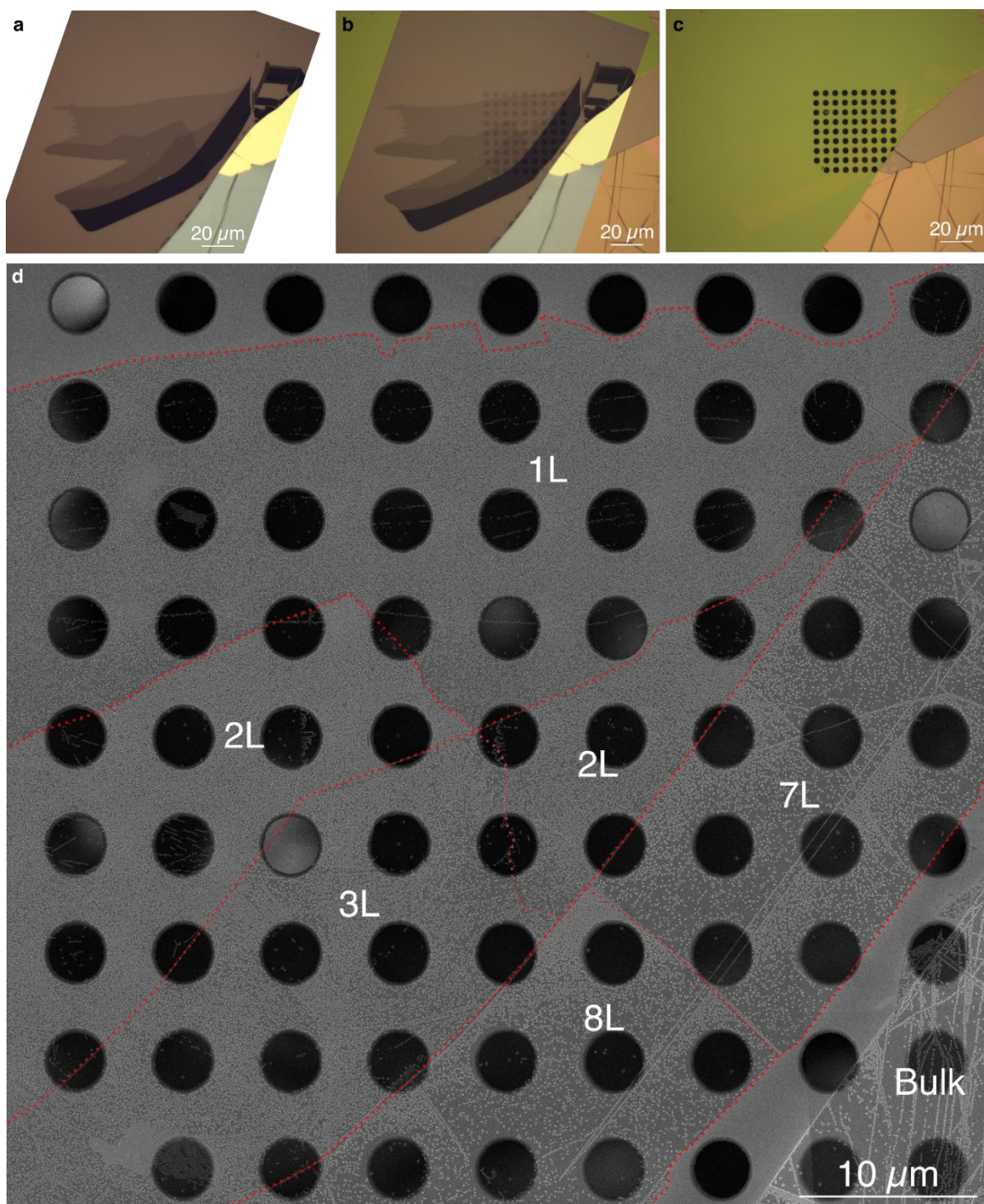


Figure S2: Overview of the sample with square, dark blue data points in Fig. 2c. (a) Optical image of the Gr crystal before transfer. (b) The optical image overlaid the sample shown in (c) and made transparent. (c) Optical image of the sample after transfer of the Gr. (d) Montage of SEM images of the sample. The square dark blue data points in Fig. 2c are from the sample shown in Fig. S2.

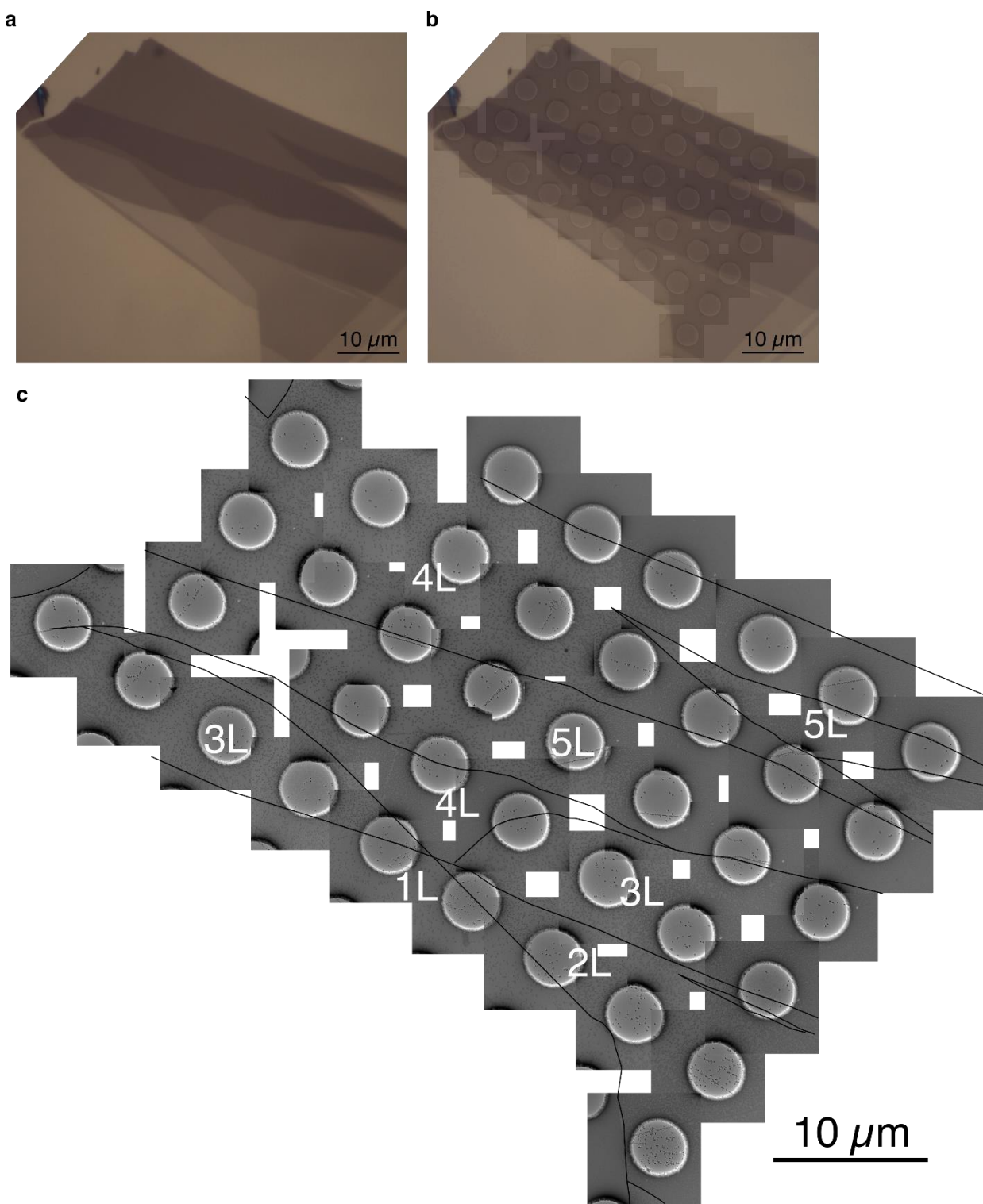


Figure S3: Overview image of the sample with round, blue data points in Fig. 2c. (a) Optical image of the Gr crystal before transfer. (b) The optical image overlaid the image shown in (c) and made transparent. (c) Montage of TEM images of the sample.